Low velocity impact on CFRP plates with compressive preload: Test and modelling

S. Heimbs, S. Heller, P. Middendorf, F. Hähnel, J. Weisse

Accepted Manuscript

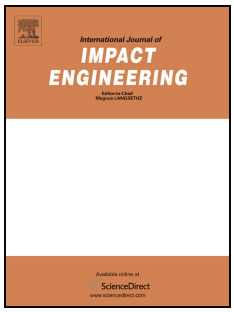

Title: Low velocity impact on CFRP plates with compressive preload: Test and modelling

Authors: S. Heimbs, S. Heller, P. Middendorf, F. Hähnel, J. Weiße

PII: S0734-743X(09)00079-7

DOI: 10.1016/j.ijimpeng.2009.04.006

Reference: IE 1774

To appear in: *International Journal of Impact Engineering*

Received Date: 25 December 2008

Revised Date: 15 April 2009

Accepted Date: 20 April 2009

Please cite this article as: Heimbs S, Heller S, Middendorf P, Hähnel F, Weiße J. Low velocity impact on CFRP plates with compressive preload: Test and modelling, International Journal of Impact Engineering (2009), doi: 10.1016/j.ijimpeng.2009.04.006

Low velocity impact on CFRP plates with compressive preload: Test and modelling

S. Heimbs [a*], S. Heller [b], P. Middendorf [a], F. Hähnel [c], J. Weiße [c]

[a] *EADS Innovation Works, 81663 Munich, Germany*
[b] *Universität Karlsruhe (TH), 76131 Karlsruhe, Germany*
[c] *Technische Universität Dresden, 01062 Dresden, Germany*

** Corresponding Author:*
Dr. Sebastian Heimbs
EADS Innovation Works
81663 Munich, Germany
Tel.+49-89-607-25884
Fax +49-89-607-23067
Email: sebastian.heimbs@eads.net

Abstract

When laminated composite materials in modern aircraft structures are subject to impact loads, they are typically not unloaded but under a certain state of prestress. Therefore, in this study the effect of a compressive preload on the low velocity impact behaviour of three different carbon fibre-reinforced plastic (CFRP) materials is investigated. An experimental test programme is documented first, including the design of a preload test device, the specimen manufacture and the results description. An increased deflection and energy absorption for composite plates with a preload of 80% of the buckling load could be observed. Non-destructive inspections showed a large extent of delaminations occurring between individual plies, being an important energy absorption mechanism. The development of numerical simulation methods for this impact scenario using the commercial explicit finite element code LS-DYNA is described in detail. The focus is on the composite material, delamination and preload modelling. The final simulation results showed a good correlation to the experimental data in terms of force and energy plots or the evaluated interlaminar and intralaminar damage, although these numerical results proved to be strongly influenced by simulation parameters like mesh size or the number of shell element layers.

Keywords: Low velocity impact, composite laminates, preloading, finite element modelling, delamination.

1 Introduction

Fibre-reinforced composite materials are known for their high weight-specific mechanical properties and are therefore used in numerous lightweight engineering applications, in particular in aircraft design. However, a constant concern for such laminates – much more than for similar metallic structures – are impact loads of foreign objects, which can cause internal material damage. This damage can significantly reduce the strength and it can grow under load and may be difficult to detect. Typical impact scenarios in aircraft design range from a tool dropped on the laminate surface (high mass, low velocity), over runway debris thrown up by the tires or hail (low mass, high velocity) to bird strike during flight (high mass, high velocity).

The impact behaviour of composite laminates has been treated extensively in the technical literature. A comprehensive overview on this topic is given by Abrate [1]. However, nearly all studies are concerned with

impact loads on unloaded composite materials. But with regard to aircraft structures, it is rather unlikely that the impacted surface is unloaded. The composite structure may be subject to compressive, tensile or shear loads in the operational environment. Therefore, knowledge of the effect of preloading on the impact behaviour of composite laminates is of significance, since the damage development can be drastically different. Only very few studies in the literature cover this topic.

Analytical investigations were performed by Sun and Chattopadhyay [2], Malekzadeh et al. [3], Khalili et al. [4] and Choi [5]. They all come to the conform results that under tensile preloading the contact force is increased and the contact time as well as the deflection are reduced compared to the impacted unloaded plate. These results were confirmed by the experimental tests of Mitrevski et al. [6] on glass fibre-reinforced (GFRP) composites.

Besides these GFRP laminates, most papers deal with experimental investigations of the influence of preloading on the low velocity impact behaviour of carbon fibre-reinforced composites (CFRP). And here, in particular, uniaxial and biaxial tensile preloading is investigated, as by Butcher [7], Butcher and Fernback [8], Sankar and Sun [9], Avva et al.[10], Phillips et al. [11], Park [12], Nettles et al. [13], Herszberg et al. [14], Kelkar et al. [15], Mines et al. [16] and Whittingham et al. [17]. The result of these studies is the tensile preload affecting the failure behaviour and failure modes. Garcia-Castillo et al. [18] performed a comparable investigation for high velocity impact loads. Sharma [19], Mines et al. [20] and Malekzadeh et al. [3] also included composite sandwich structures with foam or honeycomb cores in their studies.

The stress situation in the lower aircraft fuselage during take-off, when it is likely to be exposed to impacting stones propelled by the tires, is a compressive stress state. The impact behaviour under such compressive preloads is addressed in even fewer papers. This preloading condition is yet more complex because plate buckling becomes an issue for relatively thin composite structures. The investigations of Starnes et al. [21], Nettles and Lance [22], Robb et al. [23], Tweed et al. [24], Chiu et al. [25] and Zhang et al. [26] include such compressive preloads.

Besides pure experimental investigations on the impact behaviour of composite laminates, numerical finite element (FE) simulations play an increasingly relevant role in engineering development. Validated simulations not only allow for a detailed analysis of stress distributions and damage progression in the laminate during the impact event but also enable efficient parameter studies with respect to geometries, loading conditions or laminate configurations. For impact simulations as a transient loading, FE codes based on an explicit time integration scheme are typically used, which are characterised by small time step intervals. On the other side, the preloading happens on a static basis, making implicit calculations more appropriate. Therefore, the combination of preloading and impact loading requires special numerical strategies. FE simulations of low velocity impacts on preloaded composite structures have first been addressed by Sun and Chen [27]. However, just like in the work of Tweed et al. [24] and Mines et al. [20], who used the commercial explicit code LS-DYNA, no detailed information on the preload modelling are given. Kelkar et al. [28] bring forward the argument that their static and dynamic tests led to the same results. As a consequence, they considered the impact as a static loading and combined the preloading and impact simulation in an entirely implicit calculation with the commercial software ANSYS. Zhang et al. [26] used the in-house FE package FE77 and performed a completely explicit simulation utilising dynamic relaxation for the preloading. Mikkor et al. [29] as well as Pickett et al. [30] used the commercial explicit code PAM-CRASH. Especially in the latter paper a detailed description of the preloading modelling is given, which is performed as a part of the explicit simulation by stretching the composite plate directly before the impact load.

The aim of the current paper is to get a deeper insight into the influence of compressive preloads on the low velocity impact behaviour of CFRP plates. On the one hand, this is done by experimental impact test series on unloaded and preloaded specimens, which involves the design of a special specimen fixture allowing for compressive preloads. On the other hand, numerical techniques are evaluated to adequately simulate the preloading and impact event in the commercial FE code LS-DYNA, with the focus on the composite material, delamination and preload modelling.

2 Materials & manufacturing

In this study three different carbon fibre-reinforced epoxy (CF/EP) materials were investigated with a difference in their manufacturing process and laminate stacking sequence. Within this paper they are referred to as material type *A*, *B* and *C* and are specified as follows:

- *Type A*: Non-crimp fabric (NCF) in a symmetric, quasi-isotropic lay-up with 24 plies: $[-45°/0°/45°/90°]_{3s}$, Fig. 1a
- *Type B*: Prepreg tape in a symmetric, quasi-isotropic lay-up with 24 plies: $[-45°/0°/45°/90°]_{3s}$, Fig. 1b
- *Type C*: Prepreg tape in a symmetric lay-up with preferred 0°-direction and 24 plies (50/33/17 lay-up: 50% 0° plies, 33% ±45° plies and 17% 90° plies): $[0°/45°/0°/-45°/0°_2/45°/0°/-45°/90°_2/0°]_s$.

The quadraxial NCF (type *A*) from the manufacturer Saertex, made from 12K HTS carbon fibres, was used with Hexcel's RTM6 epoxy resin in a vacuum assisted process (VAP) to fabricate the CFRP plates in an autoclave at a curing temperature of 180°C. The cured plates had a mean thickness of 3.2 mm with a standard deviation of 0.08 mm and a fibre volume fraction of 51%.

In contrast to this liquid resin infusion process, in the prepreg material (type *B*, type *C*) from the manufacturer Cytec the unidirectional 12K HTS carbon fibres were already pre-impregnated with a 977-2 epoxy matrix. The prepreg tape plies were stacked according to the target fibre orientation angles and were cured in an autoclave at 180°C and 7 bar. The resulting average cured plate thickness was 2.7 mm with a standard deviation of 0.11 mm. The fibre volume fraction was 65%. An overview of the mechanical properties of the NCF and prepreg material , based on technical data sheet values of the manufacturer and adapted to the actual fibre volume contents, is given in Tab. 1 and Tab. 2. Any strain rate dependency of those properties is neglected due to the relatively low deformation speeds occurring in this low velocity impact study.

A diamond saw was used to cut out the final test specimens with a size of 400 mm x 150 mm. 2 mm thick tapered GFRP tabs with a width of 50 mm were bonded onto both sides of these specimens, reducing the free specimen length to 300 mm (Fig. 2). Both specimen ends were ground parallel to ensure a uniform lengthwise compressive load distribution. These specimen dimensions are much smaller and thicker compared to a commercial aircraft skin panel within the frames and stringers. However, the boundary conditions in this generic study were not chosen to represent a real aircraft impact scenario but to limit the complexity of testing and modelling and to achieve higher in-plane compressive loads without the occurrence of plate buckling.

A total of six strain gauges were applied on each preloaded specimen, five on the upper and one on the lower surface, see Fig. 2. The locations of these strain gauges were selected to give valuable information with respect to the following topics: if the target preloading is met, if a uniform load distribution in length and width direction of the plate is achieved and if plate buckling occurs under the compressive preload.

3 Experimental testing

The low velocity impact testing was conducted on a Dynatup 8250 drop tower facility. The CFRP plate had to be positioned under this drop tower and should also be preloaded in compression. Therefore, a special specimen fixture was designed and fabricated that allows for a specific uniaxial compressive preloading.

3.1 Specimen fixture and pre-loading device

For the lengthwise compressive preload introduction two parallel steel plates with ground surfaces were used. To achieve a fixed support of both ends of the CFRP plates, two clamping jaws were mounted on each end. The lateral sides of the plate were only simply supported with a special support inhibiting translational movements in vertical direction but allowing for horizontal translations during the preloading and rotations during the impact load. The final specimen fixture is shown in Fig. 3.

One end of this fixture was mounted to the base of the drop tower, while the other end was connected to a compression device with two hydraulic cylinders. With these cylinders the preloading force was applied to the specimen. To control the preloading both the compression force and the strain values from the specimen's strain gauges were recorded.

3.2 Low velocity impact test conditions

For all impact tests in this study a hemispherical steel impactor with a diameter of 1 in. (25.4 mm) and a mass of 1.85 kg was used (Fig. 4). The clamping conditions of the CFRP plates include a fixed support of the longitudinal ends and a simple support of the lateral sides, as illustrated before.

All three materials were tested with and without preloading. To limit the complexity of this study, a reference energy level of 40 J was chosen. Since the impactor mass was constant, this corresponds to an impact velocity of 6.5 m/s. Few additional tests with material type *B* were conducted with 30 J.

3.3 Compressive preloading conditions

The difficulty of compressive preloading is the risk of initial plate buckling as a stability failure of the relatively thin specimens under in-plane compression. The aim of this study was to avoid initial buckling and only to impact plates, which show no initial deflections. On the one hand this limits the amount of prestrain to a moderate level and affects the evaluation of the preload effect, but on the other hand the complexity of this investigation is reduced, especially with respect to the numerical modelling. The buckling loads of the respective specimen plates of type *A*, *B*, and *C* were first estimated by an analytical buckling analysis and implicit FE buckling analyses. But finally the real buckling load was determined experimentally by compressing calibration plates and evaluating the strain gauge data. The occurrence of plate buckling could be detected by a change in the strain values with respect to the first or second buckling mode. Afterwards, the in-plane compression was reduced to 80% of the detected buckling load. This corresponds to a prestrain of 1800 με for material type *A*, 1100 με for material type *B* and 670 με for material type *C*. However, these are the mean values of the maximum prestrain of the individual specimens' strain gauge data. The prestrain distribution was not ideally uniform over the whole specimen as a result of unavoidable imperfections in the plate thickness and the parallelism of the compression supports. An overview of the impact test conditions is given in Tab. 3. Shown are mean values from three specimens for each load case.

3.4 Damage evaluation by non-destructive inspection

Ultrasonic inspections are a well-established method for non-destructive evaluations of composite material damage and delaminations and were also adopted in this study. A Hillger USPC 3000 device was used, which is based on the impulse echo principle with the scanning head being both transmitter and receiver of the ultrasonic signal. If cracks or defects are present inside the specimen, a reflection is generated that is detected and visualised in a B-scan (sectional view) or C-scan (top view) image.

3.5 Test results

The results of the impact tests on unloaded and preloaded CFRP plates are summarised in Tab. 3 and in Fig. 5 and Fig. 6 in terms of time-dependent plots of impact force $F(t)$, energy $E(t)$ and plate deflection $s(t)$. The energy is computed here from the initial kinetic energy $E_{kin}(t_0)$ of the impactor, its mass m_{imp} and velocity $v(t)$. A photoelectric sensor was used to measure the initial velocity $v(t_0)$ before impact.

$$E(t) = E_{kin}(t_0) - \frac{1}{2} m_{imp} \left[v(t_0) + \Delta v(t) \right]^2 \tag{1}$$

with

$$\Delta v(t) = g \cdot t - \frac{1}{m_{imp}} \int_0^t F(t) dt \,. \tag{2}$$

The deflection $s(t)$ is calculated by double integration of the impact force

$$s(t) = \frac{1}{2} g \cdot t^2 + v(t_0) \cdot t - \frac{1}{m_{imp}} \int_0^t \int_0^t F(t) dt \,. \tag{3}$$

In general, the force level increases slowly in the beginning, which is the result of an oscillation of the plate after first contact with the impactor. When the plate swings back upwards the contact force increases steeply. After the point of maximum deflection, the force level decreases to zero again. The energy curves increase continuously to a maximum and fall to a certain level. This residual value is an indicator for the absorbed energy, which is not transferred to the impactor as elastic springback. If the plate behaved completely elastic without failure and neglect of friction losses, the energy curve would return to zero again. The deflection curve has a parabolic shape and is shown here in the positive quadrant.

The test results of all three materials indicate that the compressive preloading leads to an increased deflection of the CFRP plates and therewith to a higher extent of material damage. More energy is absorbed and less energy is returned as elastic springback compared to the unloaded plates. The increased damage can especially be seen in the ultrasonic C-scan images in Fig. 6. In general, the propagation of delaminations is higher for the preloaded specimens. Delaminations occur between several plies across the thickness, each having a dumbbell shape and orientation depending on the respective fibre orientation angle. From the top view this leads to a nearly circular shape for the quasi-isotropic prepreg specimens of material type *B* and a rather oval shape for type *A* and *C*. The marginal difference in the delaminated area between 30 J and 40 J for type *B* is in correlation with experimental findings by Avery and Grande [31]. They also impacted 24-ply CF/EP plates and found the total damage area detected by ultrasonic inspection to increase almost linearly for energies up to 30 J. No further increase was detectable until approximately 40 J, then it increased again. This was attributed to the introduction of fibre breakage as an additional damage mode between 30 and 40 J. Also in the current study the appearance of fibre cracking and blow-out of 45° plies on the back side of the plate was observed only for the 40 J specimens, which

is most clearly visible in the ultrasonic runtime images in Fig. 7. Here the different shades of grey indicate the different depths of the delaminations.

The comparison of the test results in Tab. 3 for the prepreg material types *B* and *C*, which only differ in the stacking sequence, shows that the maximum plate deflection is slightly lower for the quasi-isotropic specimens of type *B*. Also the shape of the delaminated area in Fig. 6 is different. This results from the fact that delaminations do not arise between layers of similar fibre orientation. In material type *B* with the lay-up $[-45°/0°/45°/90°]_{3s}$ a doubling of two similar layers occurs only in the midplane, leaving 22 ply interfaces for possible delaminations. The stacking sequence of type *C* $[0°/45°/0°/-45°/0°_2/45°/0°/-45°/90°_2/0°]_s$ has five doublings and only 18 potential delamination interfaces. It is known from [31] that if the creation of a delamination at a particular interface is not favourable then larger delaminations tend to occur at those interfaces, where the creation is favourable, absorbing the impact energy. This may explain the larger extent of delaminations in material type *C*, which reduce the plate's stiffness more significantly and lead to a higher deflection compared to type *B*.

The results in Tab. 3 also indicate that the NCF material type *A* absorbs considerably more energy than the prepreg material. This phenomenon may be ascribed to the lower strength properties in Tab. 2, which result from the lower fibre volume fraction, more ondulations (see Fig. 1) and lower matrix properties of RTM6 resin compared to 977-2 (the fibres are the same). Because the polyester yarn, which is used to fixate the carbon fibre non-crimp fabric, can be the origin of failure or distorts the fibre orientation and leads to resin nests, the properties of NCF material are in general lower than for unidirectional prepreg. In this material intralaminar failure occurs earlier at a lower internal stress state, which is proved by the lower impact force level in Fig. 5 compared to the prepreg material. A higher amount of impact energy is therefore absorbed by internal material damage. The specimens of type *A* showed the highest amount of fibre cracking and fibre blow-out on the back side of the plates in this study. The delamination failure for the NCF plates is limited to the five interfaces between the fixed quadraxial ply packages, because the fixating polyester yarn acts as a reinforcement in thickness direction and impedes delaminations. This can be seen in the ultrasonic B-scan images in Fig. 8. In these cross-sectional views through the impacted plates the depths of the delaminations from the upper surface can be visualised. However, only the first delaminations from the top are visible, the ones below are in the shadow and cannot be detected. But still a large difference between material type *A* and *B* is obvious in Fig. 8. While in the prepreg material type *B* delaminations can occur between any ply, they are limited to the few quadraxial package interfaces in material type *A*. As a consequence, larger delaminations are created here.

The variation of the in-plane loading during the impact can be evaluated from the strain gauge data. In general, the strain level varies during the impact with respect to the strain gauge position, e.g. the strain gauges close to the impact location on the top surface, which is the compression side under bending, show increased compression strains. After the impact, the strain gauges indicate a remaining buckling deformation for types *A* and *C*, while the plates of type *B* return to their initial state.

Summarising the experimental results of the low velocity impact tests on CF/EP plates with energies of 40 J, it can be stated that both intralaminar (fibre breakage and matrix failure) and interlaminar (delamination) failure occur in the composite material with the compressive preload increasing the amount of damage and energy absorption. Therefore, the emphasis in the development of impact simulation models must be placed on intralaminar and interlaminar failure and preload modelling.

4 Modelling & simulation

In order to investigate if the experimentally determined failure behaviour of CFRP plates with compressive preload under low velocity impact loads can be represented in a numerical simulation, modelling methodologies of the composite material failure, delaminations and preload have been investigated. For this purpose the commercial explicit finite element software LS-DYNA was used.

4.1 Model development

The development of the FE model for the low velocity impact simulations in LS-DYNA involves the modelling of the composite material including intralaminar failure and delamination failure, the modelling of the preload and the modelling of the impactor with adequate contact definitions. These topics are addressed as follows.

4.1.1 Composite material modelling

The composite plates consist of 24 plies of unidirectional CF/EP. As the plates' length and width dimensions are large compared to the thickness, a 2D modelling approach with shell elements is appropriate. In aircraft engineering shell models are standard because almost all structures in aircraft design are thin-walled, although in this transverse impact load case stresses in thickness direction may exist. However, it would not be adequate to investigate a 3D modelling approach in this study, which might increase accuracy, but is of minor relevance for the engineering practice due to the high computational cost and inefficiency. The linear-elastic composite material model Mat54 for shell elements in LS-DYNA, based on the failure criteria by Chang and Chang [32] was adopted. The elastic material behaviour of the individual ply is calculated based on the input of the Young's modulus, shear modulus and Poisson's ratio (see Tab. 1). Damage occurs as soon as one of the four criteria by Chang/Chang is met. Four criteria are distinguished, representing tensile and compressive failure in the fibre and matrix direction of the unidirectional ply (Fig. 9). A special criterion for shear failure is not implemented. The interaction of shear stresses is included in the failure criteria instead.

Tensile failure, fibre direction:

$$e_{f,t}^2 = \left(\frac{\sigma_1}{XT}\right)^2 + \beta\left(\frac{\tau_{12}}{SC}\right)^2 - 1 \begin{cases} \geq 0 & failure \\ < 0 & elastic \end{cases} \tag{4}$$

Compressive failure, fibre direction:

$$e_{f,c}^2 = \left(\frac{\sigma_1}{XC}\right)^2 - 1 \begin{cases} \geq 0 & failure \\ < 0 & elastic \end{cases} \tag{5}$$

Tensile failure, matrix direction:

$$e_{m,t}^2 = \left(\frac{\sigma_2}{YT}\right)^2 + \left(\frac{\tau_{12}}{SC}\right)^2 - 1 \begin{cases} \geq 0 & failure \\ < 0 & elastic \end{cases} \tag{6}$$

Compressive failure, matrix direction:

$$e_{m,c}^2 = \left(\frac{\sigma_2}{2SC}\right)^2 + \frac{\sigma_2}{YC}\left(\frac{YC^2}{4SC^2} - 1\right) + \left(\frac{\tau_{12}}{SC}\right)^2 - 1 \begin{cases} \geq 0 & failure \\ < 0 & elastic \end{cases} \tag{7}$$

Here *XT* and *XC* are the strength values for tension and compression in fibre direction, *YT* and *YC* in matrix direction. *SC* is the shear strength. The strength values were taken from Tab. 2. The parameter β can be used to scale the shear stress interaction in the fibre tensile failure criterion. $\beta=1$ yields the Hashin criterion, which overestimates the shear stress interaction as stated by Schweizerhof et al. [33]. $\beta=0$, on the other hand, yields the

simple maximum stress criterion without interaction. In this study a value of $\beta=0.04$ was used. As known from other impact studies, the matrix tensile and fibre tensile failure criteria play the most significant role for the low velocity impact behaviour of composite laminates.

In addition to these stress-based criteria, failure strains can be defined as well. When these failure strain parameters in Mat54 are used, the stress level after meeting the Chang/Chang criteria is kept at a constant level until the failure strains are reached. Then the respective layer is assigned with zero stiffness properties. This post-damage behaviour is based on the theory of Hahn and Tsai [34], who found a better correlation of the model with experimental data, if the post-damage stress level of the unidirectional ply is kept constant until the whole laminate fails, instead of setting it to zero immediately.

Inside one shell element a number of sub-layers can be defined in thickness direction, representing the laminate lay-up, which is referred to as a 'layered shell' modelling approach. In this study, each single ply was defined by one integration point with the respective ply thickness and fibre orientation angle. Once all single layers of the shell element have failed, the whole element is eroded, i.e. deleted from the calculation. Underintegrated four-node shell elements of the type Belytschko-Tsay [35] with a stiffness-based hourglass control were used for the modelling of the composite plate. This was justified since the hourglass energy in the final impact simulations was negligible with less that 1% of the total energy, which makes the utilisation of more expensive elements with a selectively reduced or full integration unnecessary.

4.1.2 Delamination modelling

Interlaminar delamination failure as the separation of two laminate layers plays a significant role in low velocity impacts on composite plates as an energy absorption mechanism and a degradation factor of the plate's stiffness and should therefore be implemented in the simulation model. In this study, the LS-DYNA contact formulation Contact_automatic_one_way_surface_to_surface_tiebreak with the failure law option 8 [35] was used between separate shell elements. This modelling approach is referred to as a 'stacked shell' model. The contact allows for the simulation of crack propagation based on the cohesive zone model, implemented in LS-DYNA as a delamination contact by Borg [36]. After defined normal and shear failure stresses (NFLS, SFLS) are met, damage is a linear function of the distance of two points initially in contact. As soon as a defined critical crack opening (CCRIT) is reached, the contact is released and converted into a regular surface-to-surface contact preventing penetrations. The energy release rates G_{IC} and G_{IIC} for normal and shear interface failure are approximated by

$$G_{IC} = \frac{1}{2} \cdot NFLS \cdot CCRIT \tag{8}$$

$$G_{IIC} = \frac{1}{2} \cdot SFLS \cdot CCRIT \, . \tag{9}$$

The value NFLS was determined in a numerical analysis of a double cantilever beam (DCB) test. First the critical force F_{crit} and the critical crack opening displacement d_{crit}, which are necessary for the crack propagation, were calculated analytically based on the known value of G_{IC} =225 J/m² as a material constant and the following equations:

$$F_{crit} = \sqrt{G_{IC} \frac{b}{a^2} EI} \tag{10}$$

$$d_{crit} = \frac{2}{3}\frac{F_{crit}a^3}{EI} \tag{11}$$

with a as the initial crack opening length, b as the specimen width and EI as the bending stiffness. This crack opening was applied to a corresponding FE model of the DCB specimen in LS-DYNA and the resulting normal interface stress at the crack tip was evaluated under this crack opening load case, which is the value NFLS. The value CCRIT can be obtained subsequently by solving equation (8). Finally, equation (9) was used to calculate SFLS with the known value of CCRIT and G_{IIC} =640 J/m².

This study covers 24-ply CFRP laminates. If each ply is modelled as a separate layer of shell elements with 23 delamination contact formulations in-between, the model would be very expensive to calculate. Moreover, a certain minimum contact thickness has to be assured in order to avoid contact breakdown [37]. As an alternative, different models with two, three, four and six separate layers of shell elements were generated, each shell element covering a certain number of different plies as different internal integration points. For comparison reasons, a model with just one shell element and without delamination was also generated. Identical parameters NFLS, SFLS and CCRIT of the delamination contact were used for the models with two to six layers of shell elements. In this case, the latter model with five contact interfaces corresponds to the NCF material type *A*, where delaminations occurred only between the six quadraxial ply packages. Although this modelling approach is not able to cover reality by enabling delamination between each single ply of the prepreg material, it is, however, an approach to evaluate if interlaminar failure occurs at all and an additional energy absorption mechanism. An alternative delamination modelling method in a shell element model is the utilisation of cohesive elements, which was not adopted in this study.

4.1.3 Preload modelling

While the low velocity impact is a transient load case with material damage occurring in a short time period, the compressive preloading of the composite plate, on the other hand, happens on a rather static basis. To combine these two loadings in a single model, different numerical approaches have been investigated.

One way is to use the implicit LS-DYNA solver for the preloading and the explicit solver for the transient impact loading. The implicit-explicit switching functionality in LS-DYNA is straightforward and can be performed within one single input deck. With this technique, the implicit preloading calculation takes only a few seconds, making this method very efficient. However, neither the delamination contact nor the cohesive elements are implemented in the implicit solver version used in this study, making this technique inapplicable.

The other way is to use solely the explicit LS-DYNA solver, also for the preloading. To avoid oscillations, the displacement-controlled preloading should be applied within a sufficiently long time interval or by using the dynamic relaxation feature to damp nodal velocities. This method is less computationally efficient – though more stable.

In this study, the explicit solver without dynamic relaxation was used for both preloading and impact loading due to stability reasons. The displacement-controlled compressive prestress was applied in a period of 10 ms without provoking any noticeable oscillations, with the impact event lasting approx. 6 ms until springback. With respect to a slightly decreasing time step size, this corresponds to half of the total computational time ascribed to the preloading and the other half to the impact load. A further benefit in computational time might be achievable with the Initial_strain_shell and Initial_stress_shell options in LS-DYNA, which were not investigated in this

study. The other boundary conditions in the model were defined corresponding to the impact test rig, with fully constrained nodes at the longitudinal ends of the specimen and simply supported nodes at the lateral ends.

The impactor was modelled as a spherical rigid body with conventional shell elements and the rigid LS-DYNA material model Mat20 as well as a defined initial velocity. Another alternative would be the modelling of the impactor as an idealised spherical contact entity without a user-defined mesh. However, in this study this led to a significantly higher computational cost, and was therefore not applied.

4.2 Simulation results

4.2.1 Comparison between experiment and simulation

In this section the simulation results are presented and compared with the experimental data. To limit the amount of result data in this paper, only material type *B* is treated in the following sections. The general findings have been verified to be similar for the other two types *A* and *C*. Since numerous simulation parameters have a significant influence on the numerical results, one reference model is treated first. The influence of the single parameters (mesh size, number of shell element layers etc.) is discussed later. This reference model consists of three layers of shell elements with two delamination tiebreak contacts in-between and an element length of 3 mm (Fig. 10). For a comparison between experimental and numerical results, the following data were evaluated:

• Impact contact force:

While the contact force in the experiment was recorded directly by the strain gauge-based load cell, the numerical force curve was obtained by recalculating the impactor's rigid body acceleration. The results for the unloaded and preloaded case are shown in Fig. 11. The correlation between experiment and simulation is acceptable in both cases. In the beginning, the behaviour is characterised by an oscillation of the plate after first contact with the impactor, which is represented correctly by the simulation model. When the plate swings back upwards the contact force increases steeply. The further drops in the force plot result from oscillations and material damage. Despite some deviations in the curve peak values, the overall contact time matches again very satisfactorily.

• Energy plot:

The results of the energy plot are shown in Fig. 12. For the unloaded and preloaded case the experimental and numerical curves match with a high degree of accuracy. Also the final values of the absorbed energy are in good correlation.

• Interlaminar failure (delamination):

In the experiment, the delaminated area is slightly higher for the plate with compressive preload compared to the unloaded plate (Fig. 6). The diameter measures approx. 25 mm. In the simulation model an additional interface force file was written out for the visualisation of the delamination contact. Once the contact fails completely and CCRIT is reached, the respective nodal value of a failure variable changes from 1 to 0, which can be visualised in a two-coloured fringe plot in Fig. 13. Shown are the two contact interfaces with black shading around each released node. In the reference simulation model with two tiebreak contact interfaces the visualisation of the delaminated area as described above also leads to a diameter of 25-30 mm. However, is has to be kept in mind

that the comparability of the illustration in Fig. 13 and the C-scan image in Fig. 6 is limited, because the model only consists of two interfaces with possible interlaminar failure. Although the area might be similar from the top view, the real delaminations in the C-scan image are built up from numerous delaminations between more than just two interfaces. The simulation results just indicate that interlaminar failure occurs and give a rough estimation of the propagation.

• Intralaminar failure (fibre/matrix failure):

The intralaminar fibre and matrix damage could not be evaluated precisely in the test specimens but could only be analysed in the LS-DYNA simulation results by plotting the Mat54 failure variables. These variables are set from 1 to 0 if failure occurs in fibre tensile mode, fibre compressive mode, matrix tensile mode or matrix compressive mode. The simulation results of the reference model showed that the only intralaminar failure mode occurring is matrix tensile failure. The two-coloured fringe plot of this failure variable for the individual integration points across the thickness of the 24-ply laminate is shown in Fig. 14. Three stacks with eight layers can be seen, each stack representing one shell element and each layer representing one integration point across the shell's thickness. Damage starts from the bottom plies on the opposite side of the impact. This is the tensile side under plate bending and since the matrix tensile strength has the lowest value (see Tab. 2), failure occurs in matrix tensile mode. This phenomenon with higher damage in the bottom plies can both be observed for the global structure as well as for each single shell element. The extent of intralaminar damage for the preloaded model is slightly higher than for the unloaded plate.

4.2.2 Influence of element size

Since the element size is known to have an influence on simulation results, a parameter study was carried out, investigating element lengths of 1.5 mm, 2 mm, 3 mm, 4.7 mm, 6 mm and 8 mm. This study covered both models with and without a delamination contact. The results of this study showed a strong mesh dependency. This is because both the composite material failure behaviour of Mat54 and also the delamination contact are influenced by the element size, and therefore the absorbed energy varies with the element length (Fig. 15). A convergence for small elements is visible. Since the impact of the sphere is a very local load introduction, very fine meshes are necessary to cover the mechanical behaviour adequately. The parameters of the delamination contact need to be adjusted for each mesh size to obtain consistent results.

4.2.3 Influence of number of shell element layers

To evaluate the influence of the number of shell element layers in the stacked shell model, or in other words the number of delamination contact interfaces in-between, models with two, three, four and six layers of shell elements across the thickness were generated with delamination contact definitions in-between. A model with just one layer of shell elements without delamination was also compared (Fig. 16).

The corresponding energy plots from the impact simulations in Fig. 17 show a strong influence of the number of shell layers. In the model without delamination contact, the absorbed energy has the lowest value. This is because no interlaminar failure can occur in this model. Instead of that, intralaminar failure in fibre tension mode occurs in this model, which does not happen in the other models with delamination contact definitions.

In general, the more delamination contact interfaces are used, the more the bending stiffness of the plate is reduced even if no delamination occurs. In other words, the bending stiffness of a stacked shell model is lower

than the one of a layered shell model. This relation could be verified for different mesh sizes by means of bending simulations of a cantilever beam and is presumably caused by transverse shear deformations in the contact interface. The less the bending stiffness, the higher is the deflection and the material damage. In this context, the one-shell-model without delamination contact showed the highest stiffness and the lowest deflection. Therefore, an increase of the number of shell elements and delamination contacts does not necessarily bring the model closer to reality, when its stiffness behaviour is degraded in such a way.

5 Conclusions

In this study the low velocity impact behaviour of laminated carbon fibre/epoxy plates with and without compressive preloading was investigated. The experimental test series showed an increased deflection for the preloaded composite plates, which lead to a higher extent of material damage compared to the unloaded plates with delaminations as one important energy absorption mechanism. Therefore, the total absorbed energy was higher for the preloaded plates. The intralaminar and interlaminar damage was higher for the NCF material compared to the prepreg material resulting from lower stiffness and strength properties. Delaminations occurred only between the few quadraxial package interfaces, while they may occur between any ply in the prepreg material.

A further aim of this paper was to develop a model in the explicit finite element software LS-DYNA to simulate the low velocity impact behaviour of the composite plates and to investigate, if the effect of the compressive preloading can be covered adequately by the numerical model. The emphasis was on the composite material modelling, delamination modelling and preloading modelling. In this study, the composite material model Mat54 and the delamination tiebreak contact were adopted. The preloading was performed on an explicit basis, which may not be the most efficient but in this case the most stable technique. The implicit solver, which is able to reduce the computational time significantly, did not work properly with the delamination contact or alternatively with cohesive elements.

The final simulation results showed a good correlation to the experimental data in terms of force and energy plots or the evaluated interlaminar and intralaminar damage. The effect of the compressive preloading with increased energy absorption could be observed in the simulation as well. However, these numerical results proved to be strongly influenced by simulation parameters, in particular the element size and the number of shell element layers. This study showed that delamination modelling is crucial for impact simulations and delamination contacts should be included in a shell model, leading to a stacked shell modelling approach. Neglecting delaminations in a one-shell-model leads to unrealistically increased intralaminar fibre/matrix damage behaviour.

References:

1. Abrate S. Impact on composite structures. Cambridge University Press, 1998.

2. Sun CT, Chattopadhyay S. Dynamic response of anisotropic laminated plates under initial stress to impact of a mass. J Appl Mech 1975;42:693-698.

3. Malekzadeh K, Khalili MR, Mittal RK. Response of in-plane linearly prestressed composite sandwich panels with transversely flexible core to low-velocity impact. J Sandw Struct Mater 2006;8(2):157-181.

4. Khalili SMR, Mittal RK, Mohammad Panah N. Analysis of fiber reinforced composite plates subjected to transverse impact in the presence of initial stresses. Compos Struct 2007;77(2):263-268.

5. Choi IH. Low-velocity impact analysis of composite laminates under initial in-plane load. Compos Struct 2008;86(1-3):251-257.

6. Mitrevski T, Marshall IH, Thomson RS, Jones R. Low-velocity impacts on preloaded GFRP specimens with various impactor shapes. Compos Struct 2006;76(3):209-217.

7. Butcher BR. The impact resistance of unidirectional CFRP under tensile stress. Fibre Sci Technol 1979;12:295-326.

8. Butcher BR, Fernback PJ. Impact resistance of unidirectional CFRP under tensile stress: further experimental variables. Fibre Sci Technol 1981;14:41-58.

9. Sankar BV, Sun CT. Low-velocity impact damage in graphite-epoxy laminates subjected to tensile initial stresses. AIAA J 1986;24(3):470-471.

10. Avva VS, Vala JR, Jeyaseelan M. Effect of impact and fatigue loads on the strength of graphite/epoxy composites. In: Whitney JM, editor. Composite materials: testing and design (seventh conference), ASTM STP 893, 1986, p. 196-206.

11. Phillips DC, Park N, Lee RJ. The impact behaviour of high performance, ceramic matrix fibre composites. Compos Sci Technol 1990;37(1-3):249-265.

12. Park N. The impact response of composites under stress. In: Proceedings IMechE, Fibre reinforced composites, March 27-29, 1990, p. 137-143.

13. Nettles A, Daniel V, Branscomb C. The effects of tensile preloads on the impact response of carbon/epoxy laminates. In: Proceedings of the 40th International SAMPE Symposium, Anaheim, CA, 1995, p. 1019-1025.

14. Herszberg I, Weller T, Leong KH, Bannister MK. The residual tensile strength of stitched and unstitched carbon/epoxy laminates impacted under tensile load. In: Proceedings of the first Australasian congress on applied mechanics, Melbourne, Australia, 1996, p. 309-314.

15. Kelkar AD, Sankar J, Grace C. Behavior of tensile preloaded composites subjected to low-velocity impact loads. In: ASME Recent Advances in Solids/Structures and Application of Metallic Materials, PVP-Vol. 369, 1997, p. 39-46.

16. Mines RAW, Li QM, Birch RS. Static behaviour of transversely loaded CFRP laminate panels subject to in-plane tension. Strain 2000;36(2):71-80.

17. Whittingham B, Marshall IH, Mitrevski T, Jones R. The response of composite structures with pre-stress subject to low velocity impact damage. Compos Struct 2004;66(1-4):685-698.

18. Garcia-Castillo SK, Sanchez-Saez S, Barbero E, Navarro C. Response of pre-loaded laminate composite plates subject to high velocity impact. J Phys IV 2006;134:1257-1263.

19. Sharma AV. Low-velocity impact tests on fibrous composite sandwich structures. In: Chamis CC, editor. Test Methods and design allowables for fibrous composites, ASTM STP 734, 1981, p. 54-70.

20. Mines RAW, Li QM, Birch RS, Rigby R, Al-Khalil M, Tanner A. (2004): Static behaviour of pre-stressed polymer composite sandwich beams. In: Gdoutos EE, editor. Recent advances in experimental mechanics, Springer Netherlands, 2004, p. 671-682.

21. Starnes JH, Rhodes MD, Williams JG. Effect of impact damage and holes on the compressive strength of a graphite/epoxy laminate. In: Pipes RB, editor. Nondestructive evaluation and flaw criticality for composite materials, ASTM STP 696, 1979, p. 145-171.

22. Nettles AT, Lance DG. The effects of compressive preloads on the compression-after-impact strength of carbon/epoxy. NASA Technical Paper 3303, 1992.

23. Robb MD, Arnold WS, Marshall IH. The damage tolerance of GRP laminates under biaxial prestress. Compos Struct 1995;32(1-4):141-149.

24. Tweed JH, Lee RJ, Dyson RJ, Hancox NL, McCarthy JC. Impact performance of stressed composites. In: Proc. of the 7th European conference on composite materials, ECCM-7, London, UK, 1996, p. 111-116.

25. Chiu ST, Liou YY, Chang YC, Ong CI. Low velocity impact behavior of prestressed composite laminates. Mater Chem Phys 1997;47(2-3):268-272.

26. Zhang Z, Davies GAO, Hitchings D. Impact damage with compressive preload and post-impact compression of carbon composite plates. Int J Impact Eng 1999;22(5):485-509.

27. Sun CT, Chen JK. On the impact of initially stressed composite laminates. J Compos Mater 1985;19(6):490-504.

28. Kelkar AD, Sankar J, Rajeev K, Aschenbrenner RJ, Schoeppner G. Analysis of tensile preloaded composites subjected to low-velocity impact loads. In: Proceedings of 39th AIAA/ASME/ASCE/AHS/ASC Structures, Structural Dynamics, and Materials Conference, Long Beach, CA, 1998, p. 1978-1987.

29. Mikkor KM, Thomson RS, Herszberg I, Weller T, Mouritz AP. Finite element modelling of impact on preloaded composite panels. Compos Struct 2006;75(1-4):501-513.

30. Pickett AK, Fouinneteau MRC, Middendorf P. Test and modelling of impact on pre-loaded composite panels, Composites Part B, submitted for publication, 2008.

31. Avery WB, Grande DH. Influence of materials and layup parameters on impact damage mechanisms. In: 22nd International SAMPE Technical Conference, Boston, MA, 1990, p. 470-483.

32. Chang FK, Chang KY. A progressive damage model for laminated composites containing stress concentrations. J Compos Mater 1987;21(9):834-855.

33. Schweizerhof K, Maier M, Matzenmiller A, Rust W. Energy absorption with composite crash elements in frontal crash – an analysis with LS-DYNA3D. In: 11th CAD-FEM Users´s Meeting, Bamberg, 1993.

34. Hahn HT, Tsai SW. On the behavior of composite laminates after initial failures. J Compos Mater 1974;8(3):288-305.

35. LS-DYNA Keyword User's Manual, Version 971, Livermore Software Technology Corporation, Livermore, CA, 2007.

36. Borg R. Simulation of delamination initiation and growth in fiber composite laminates. PhD Thesis, Linköpings Universitet, Sweden, 2002.

37. Bala S. Contact Modelling in LS-DYNA, Part 2 – Contact Parameters: Default and Recommended Values. FEA Information International News, September 2001, p. 6-11.

Figure Captions:

Fig. 1. Micrographs of (a) material type *A* (NCF) and (b) material type *B* (prepreg).

Fig. 2. Dimensions of impact test specimens (in mm).

Fig. 3. Specimen fixture for compressive preloading.

Fig. 4. Top view of preloaded specimen in test fixture and impactor.

Fig. 5. Experimental results: Force, energy and deflection plots during low velocity impact.

Fig. 6. Experimental results: Ultrasonic C-scan images (flaw echo images) showing delaminated areas.

Fig. 7. Ultrasonic C-scan images (runtime images) of 30 J and 40 J impact.

Fig. 8. Ultrasonic B-scan images showing the distribution of delaminations in the NCF and prepreg material.

Fig. 9. Illustration of failure modes covered by the material model.

Fig. 10. Reference model for low velocity impact simulations on preloaded composite plate.

Fig. 11. Contact force plot in experiment and simulation for unloaded and preloaded prepreg plates type *B*.

Fig. 12. Energy plot in experiment and simulation for unloaded and preloaded prepreg plates type *B*.

Fig. 13. Extent of delaminations in impact simulation of preloaded plate.

Fig.14. Extent of matrix tensile failure in impact simulation of preloaded plate.

Fig. 15. Influence of element size on energy plot (here: stacked shell model with one delamination contact).

Fig. 16. Overview of different numbers of shell element layers for the composite laminate modelling.

Fig. 17. Influence of number of shell layers on energy plot (here: element size 3 mm).

Table 1

Overview of lamina elastic material properties

Material:	ρ [g/cm³]	E_{11} [GPa]	E_{22} [GPa]	G_{12} [GPa]	ν_{12}
Type *A* (NCF)	1.46	124	10.5	4.2	0.3
Type *B, C* (prepreg)	1.62	153	10.3	5.2	0.3

Table 2

Overview of lamina elastic strength properties

Material:	σ_{11}^{+} [MPa]	σ_{11}^{-} [MPa]	σ_{22}^{+} [MPa]	σ_{22}^{-} [MPa]	τ_{12} [MPa]
Type *A* (NCF)	1953	1378	67	240	61
Type *B, C* (prepreg)	2540	1500	82	236	90

Table 3

Overview of impact test conditions and results

Specimen name:	Material:	Thickness [mm]:	Prestrain [με]:	Preload [kN]:	Impact energy [J]:	Absorbed energy [J]:	Max. deflection [mm]:
A1	Type *A* (NCF)	3.2	0	0	40	22.4	12.2
A2	Type *A* (NCF)	3.2	1800	36	40	25.9	13.3
B1	Type *B* (prepreg)	2.7	0	0	40	14.0	12.2
B2	Type *B* (prepreg)	2.7	1100	23	40	17.9	13.3
B3	Type *B* (prepreg)	2.7	0	0	30	6.7	10.7
B4	Type *B* (prepreg)	2.7	1100	23	30	10.1	12.1
C1	Type *C* (prepreg)	2.7	0	0	40	12.4	13.0
C2	Type *C* (prepreg)	2.7	670	21	40	18.2	14.0

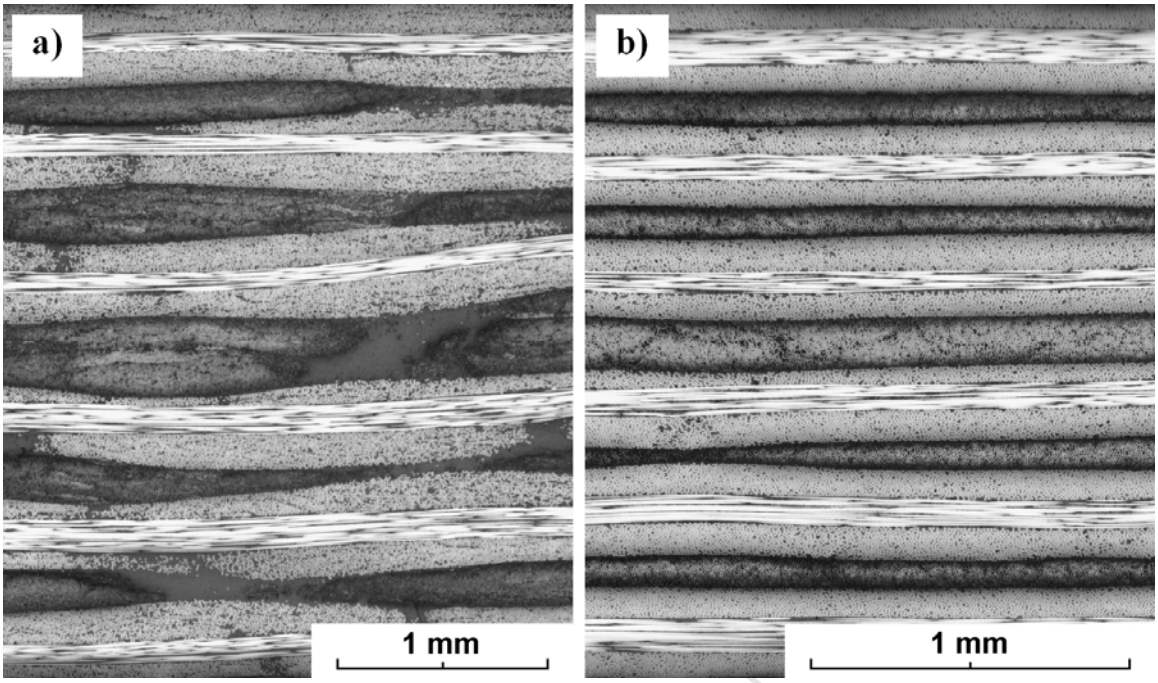

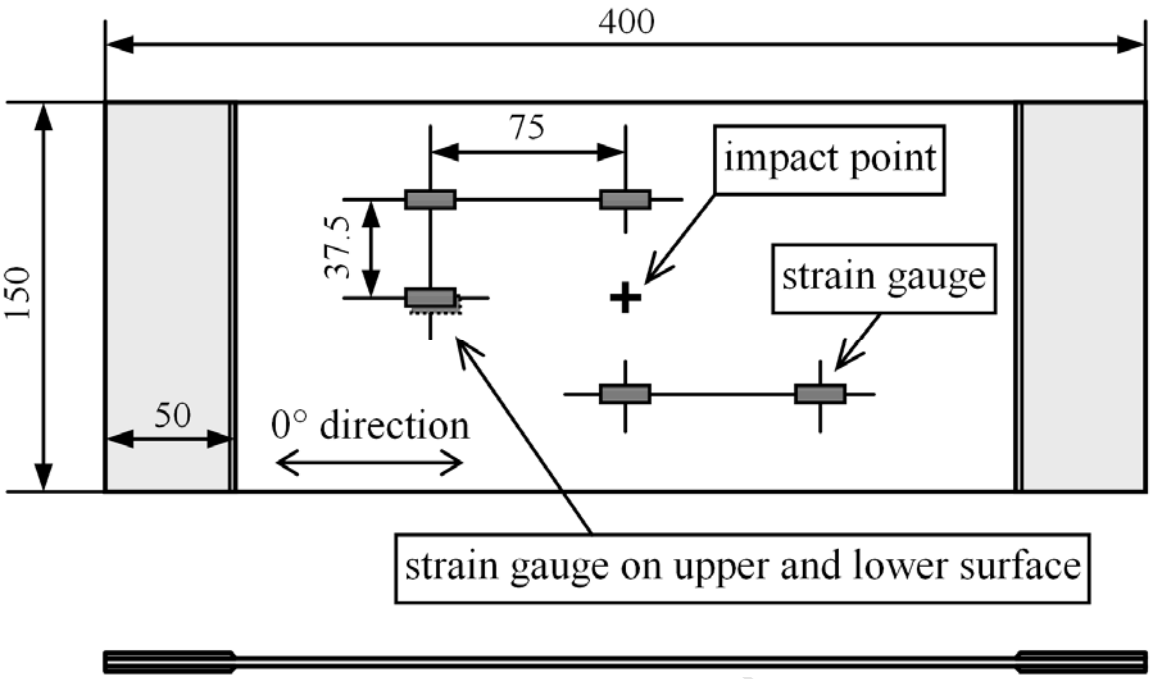

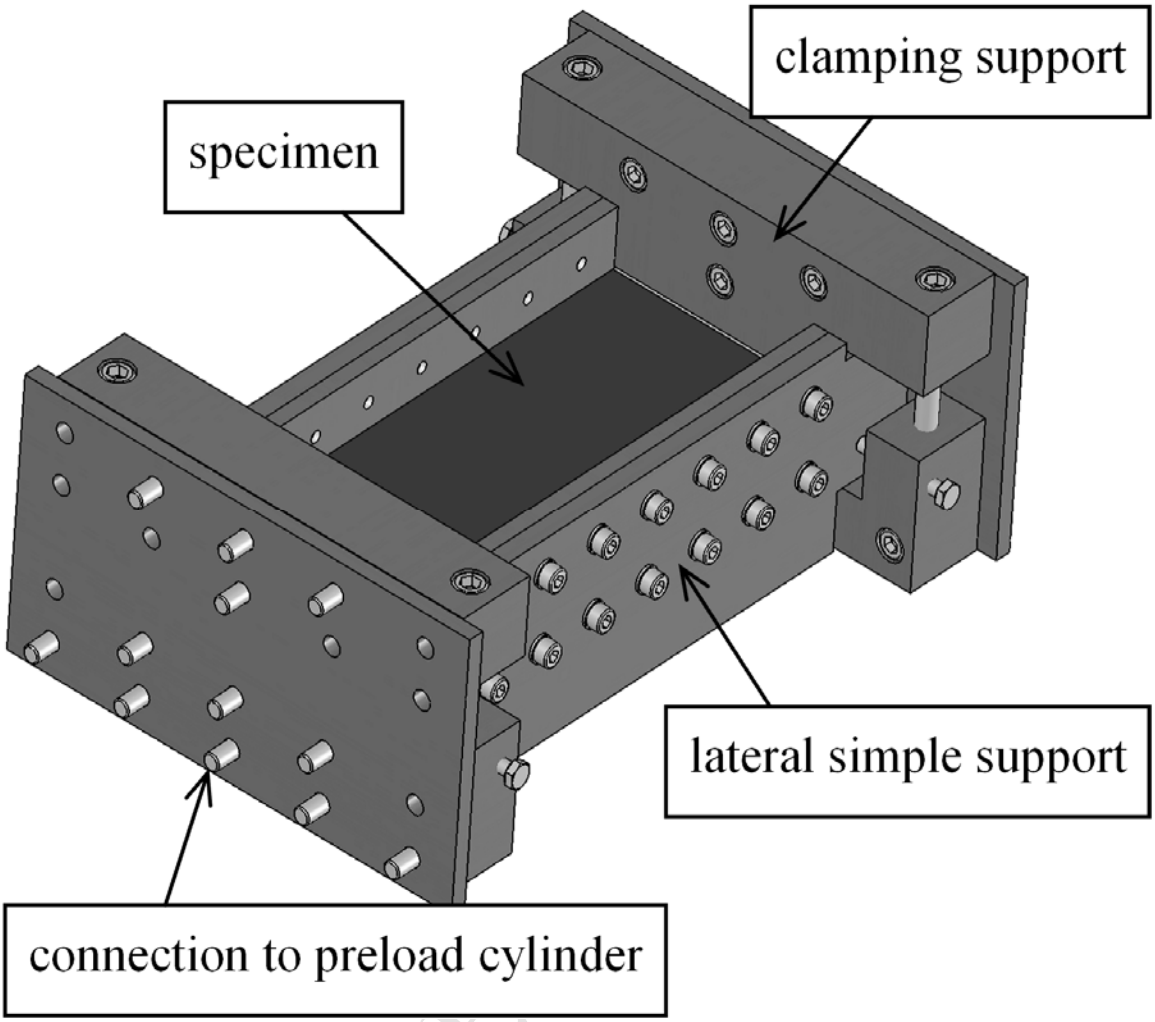
clamping support
specimen
lateral simple support
connection to preload cylinder

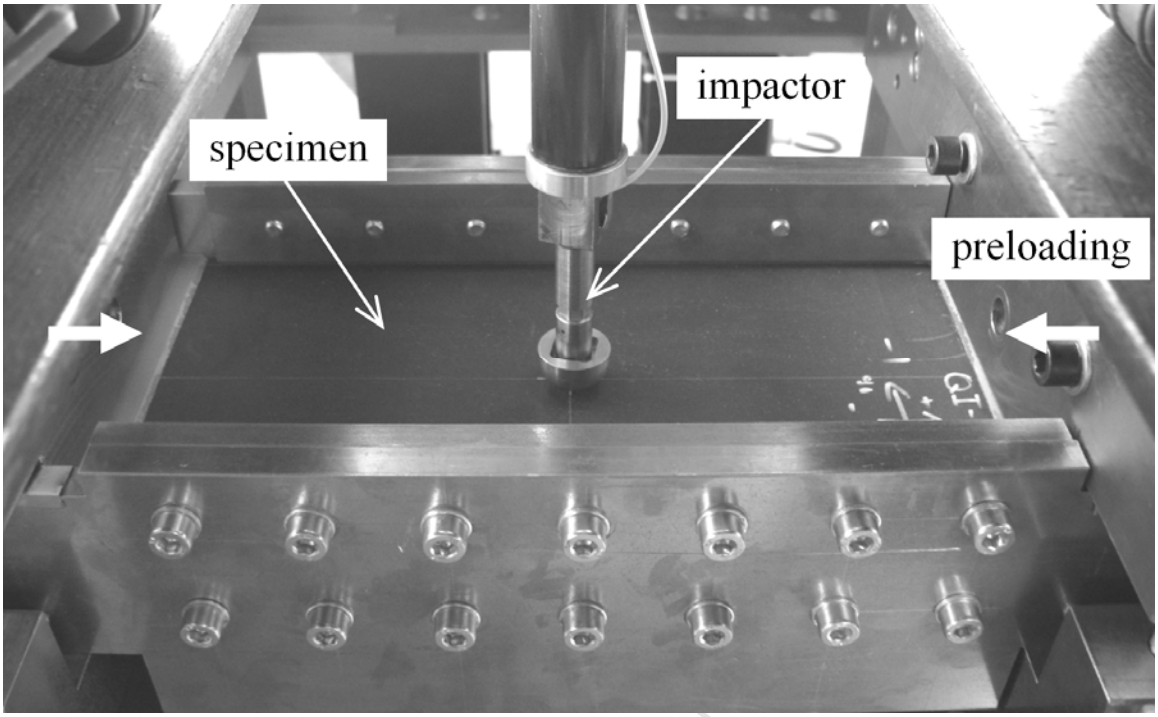

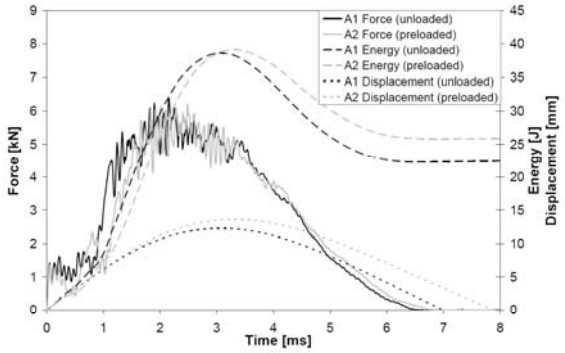

(a) Type *A* – 40 J

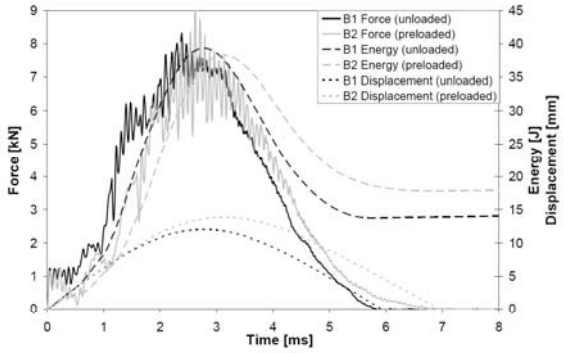

(b) Type *B* – 40 J

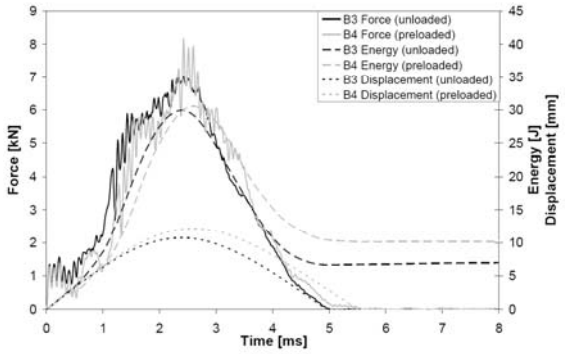

(c) Type *B* – 30 J

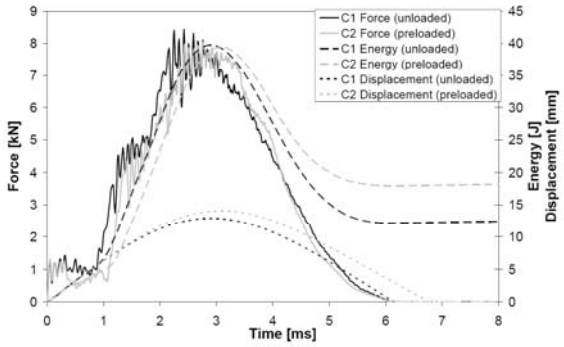

(d) Type *C* – 40 J

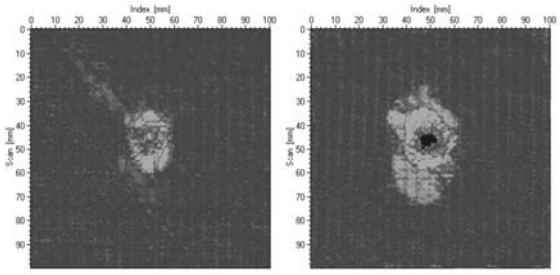

(a) Type *A* – 40 J (A1 left, A2 right)

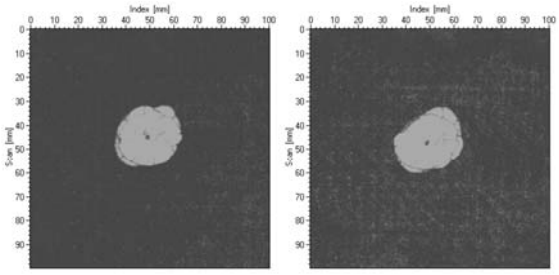

(b) Type *B* – 40 J (B1 left, B2 right)

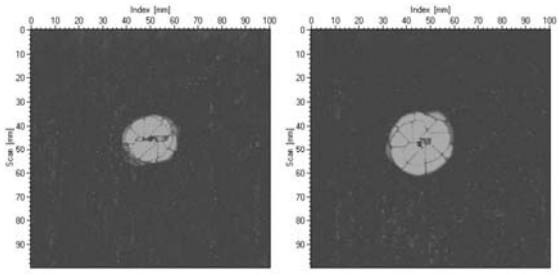

(c) Type *B* – 30 J (B3 left, B4 right)

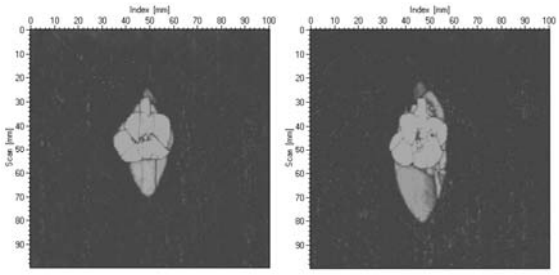

(d) Type *C* – 40 J (C1 left, C2 right)

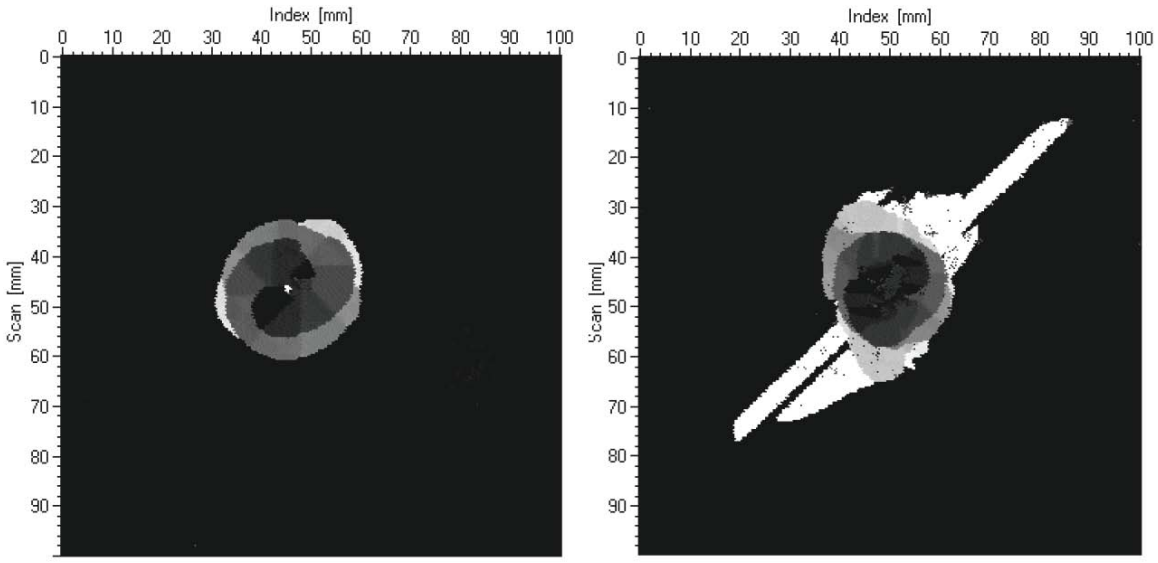

(a) B4 – 30 J (b) B2 – 40 J

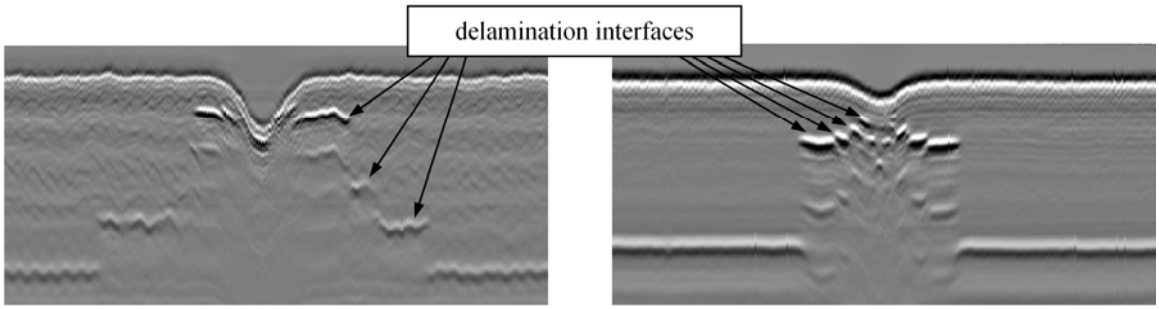

(a) type A1 (NCF)

(b) type B1 (prepreg)

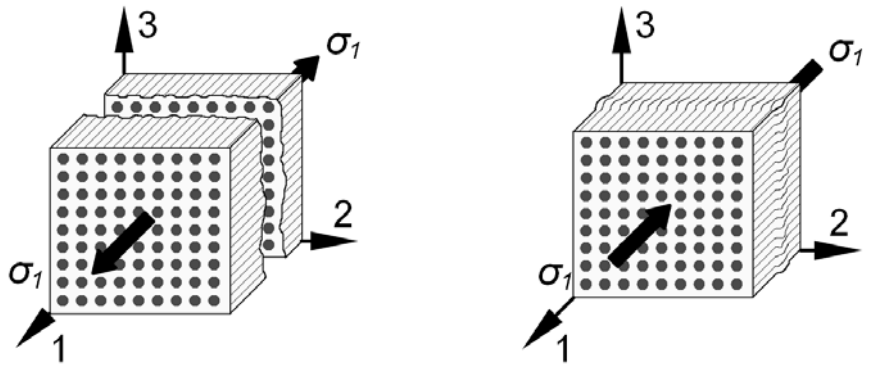

(a) Tensile and compressive failure in fibre direction:

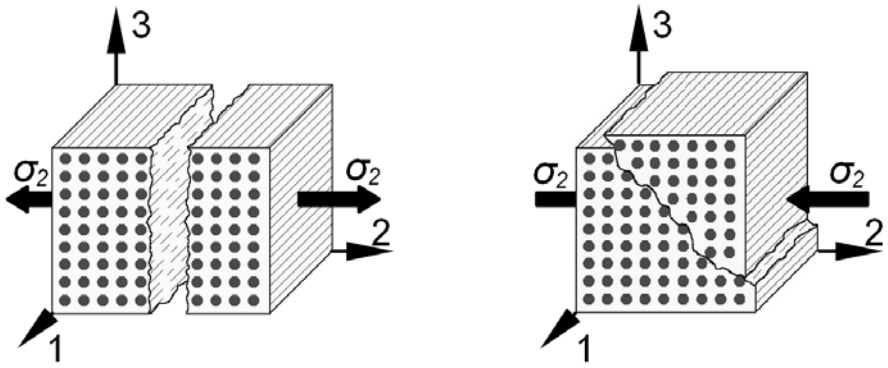

(b) Tensile and compressive failure in matrix direction:

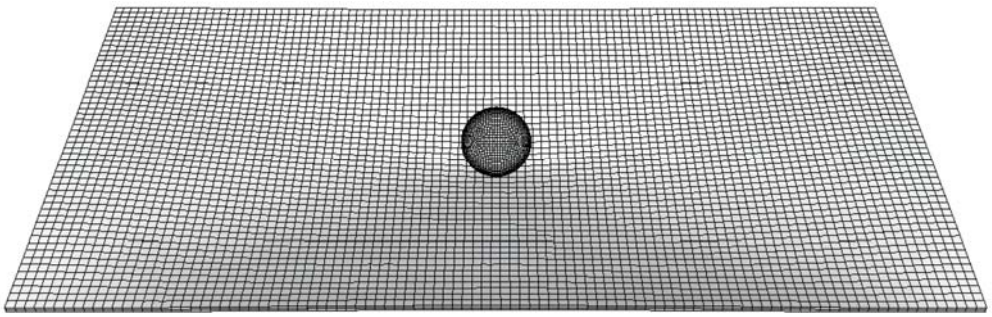

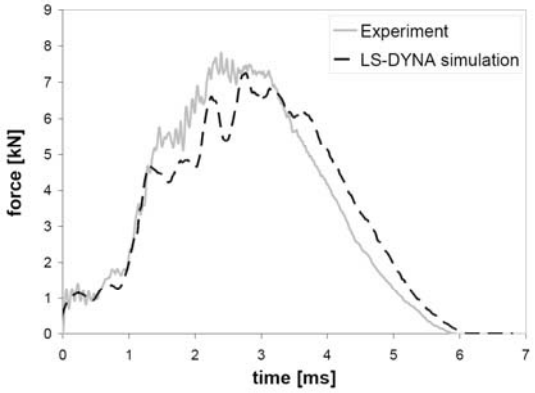

(a) Type *B1* – 40 J (unloaded)

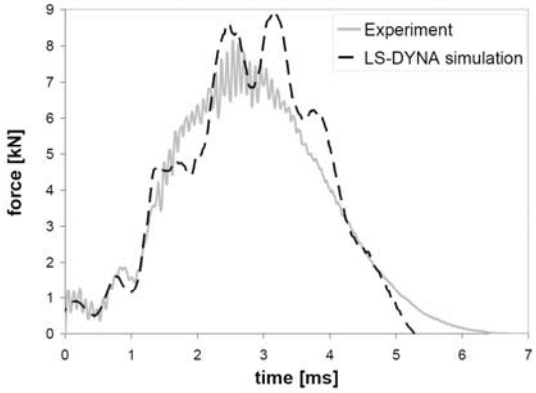

(b) Type *B2* – 40 J (preloaded)

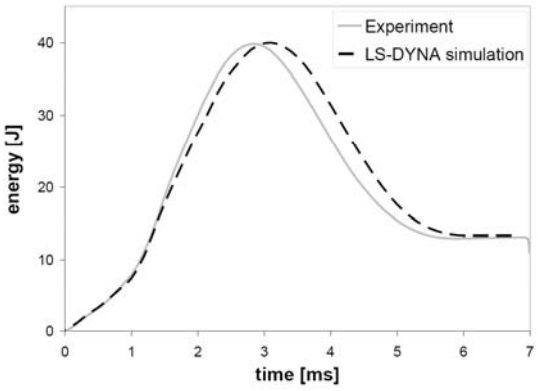

(a) Type *B1* – 40 J (unloaded)

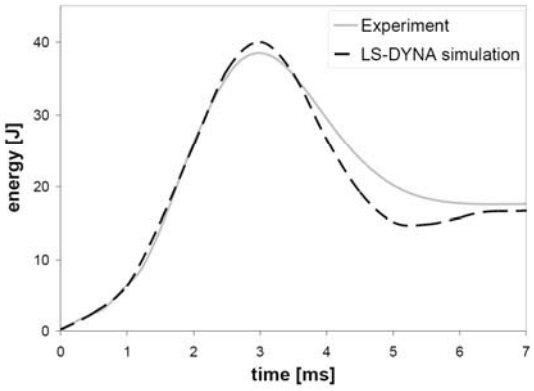

(b) Type *B2* – 40 J (preloaded)

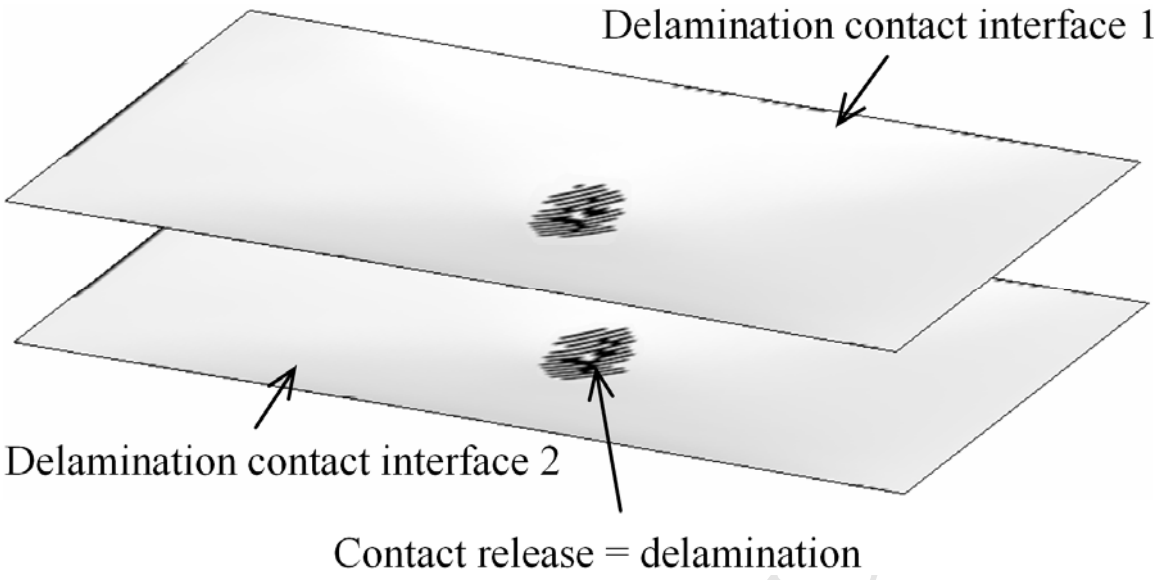

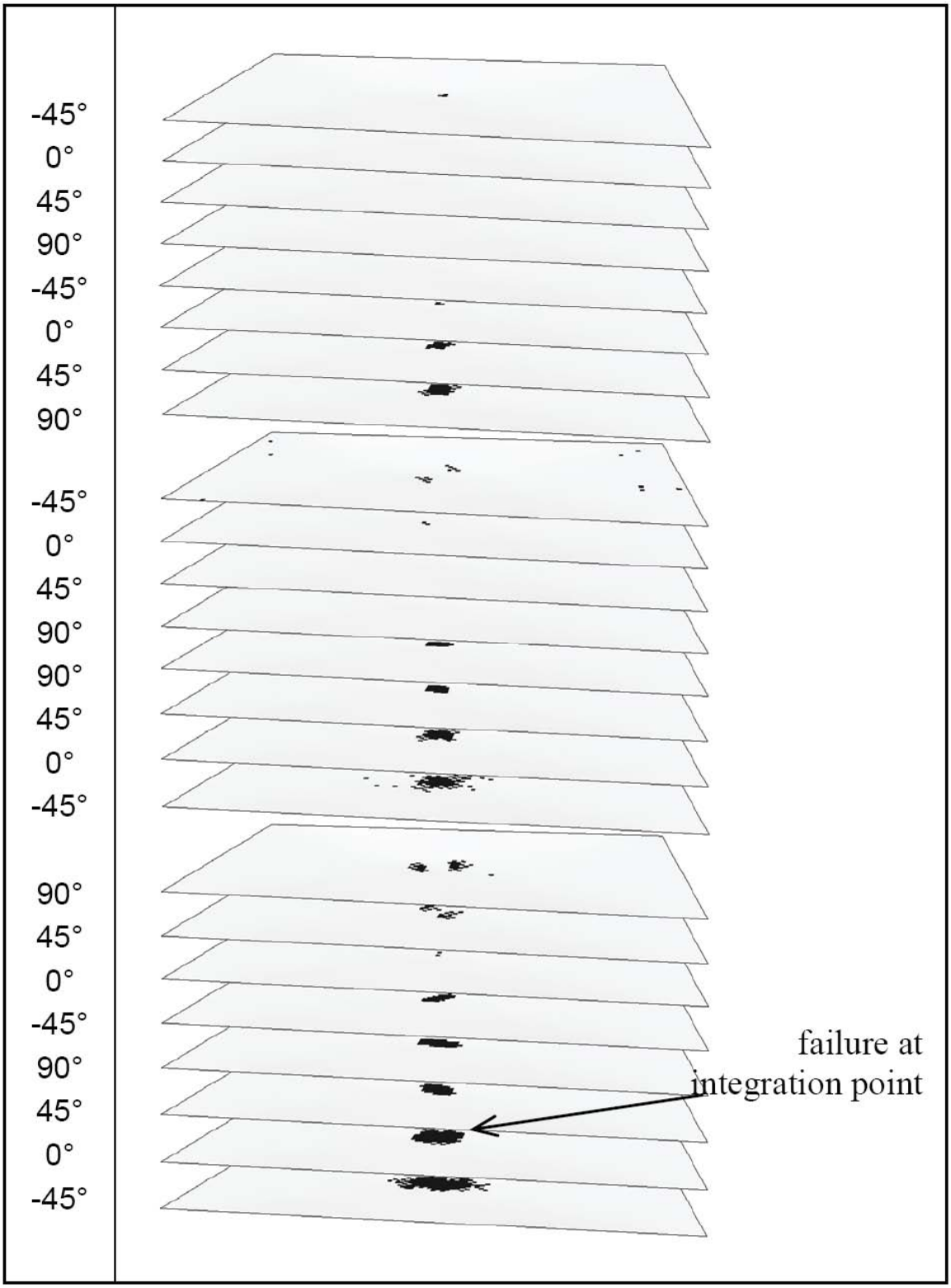
-45°
0°
45°
90°
-45°
0°
45°
90°
-45°
0°
45°
90°
90°
45°
0°
-45°
90°
45°
0°
-45°
90°
45°
0°
-45°
failure at
integration point

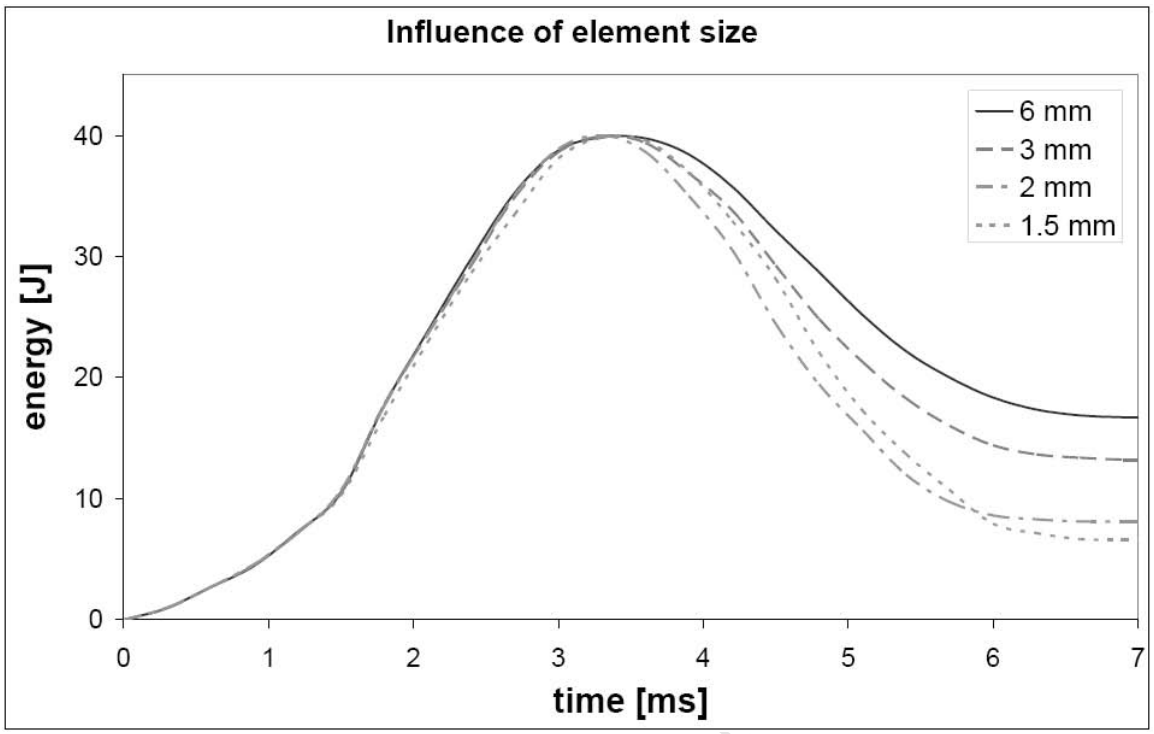
Influence of element size
6 mm
3 mm
2 mm
1.5 mm
energy [J]
0
10
20
30
40
0
1
2
3
4
5
6
7
time [ms]

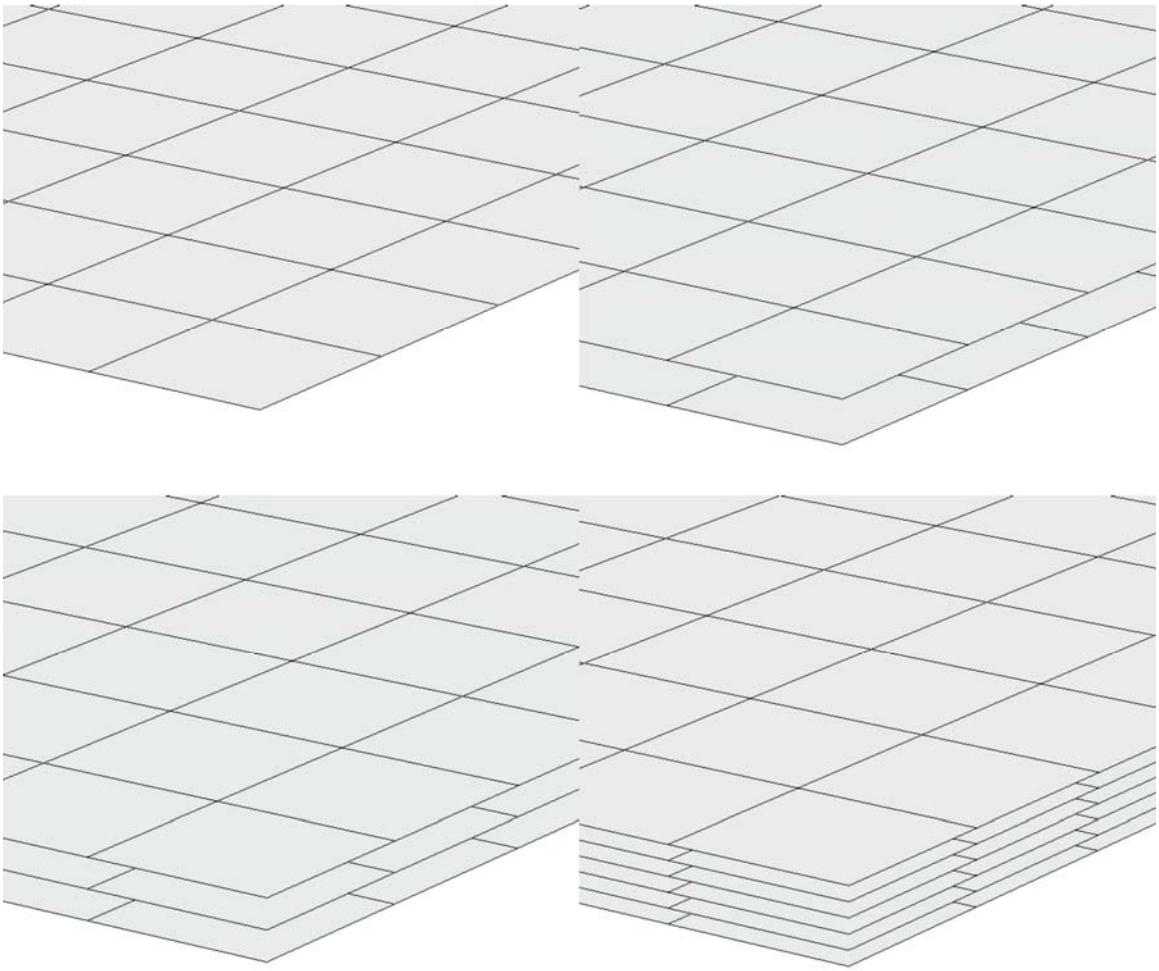

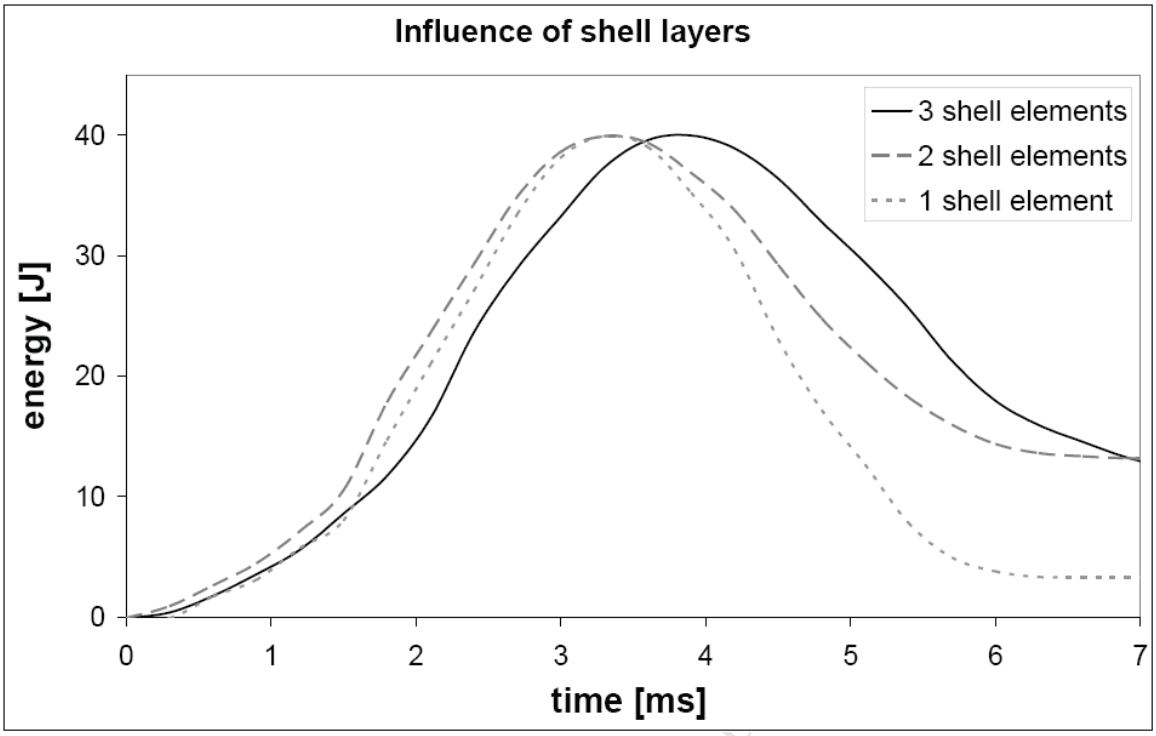
Influence of shell layers
energy [J]
time [ms]
3 shell elements
2 shell elements
1 shell element
0
10
20
30
40
0
1
2
3
4
5
6
7